frontiers in Energy Research

ORIGINAL RESEARCH
published: 22 February 2022
doi: 10.3389/fenrg.2022.840817

Tetrabutylammonium (TBA)-Doped Methylammonium Lead Iodide: High Quality and Stable Perovskite Thin Films

Amal Bouich[1,2], Júlia Marí-Guaita[1], Bouchta Sahraoui[3], Pablo Palacios[2] and Bernabé Marí[1]*

[1]Institut de Disseny I Fabricació, Universitat Politècnica de València, València, Spain, [2]Física Aplicada a Las Ingenierías Aeronáutica y Naval and Instituto de Energía Solar, Universitat Politècnica de Madrid, Madrid, Spain, [3]Institut des Sciences et Technologies Moléculaires d'Angers, University of Angers, Angers, France

This work reported the successive incorporation of tetrabutylammonium (TBA) into Methylammonium lead Iodide ($MAPbI_3$) perovskite. The thin films were characterized by X-Ray diffraction (XRD), Scanning electron microscopy (SEM), Transmittance electron microscopy (TEM), Atomic force microscopy (AFM), and UV-Visible spectroscopy. It was shown that introducing TBA increases the crystallinity, grain size, surface morphology without pin-hole, and roughness of the $MAPbI_3$ thin films. Moreover, the $MA_{(1-X)}TBA_X$ PbI_3 thin film shows better stability in a relative humidity of ~60% after 15 days than the pure $MAPbI_3$ thin film. The obtained results are hoped to be helpful for stability and improvement of the performance of the $MAPbI_3$ thin films by doping TBA cations under ambient conditions.

Keywords: $MA_{(1-X)}TBA_xPbI_3$, XRD, SEM, TEM, PL, UV-visible spectroscopy

OPEN ACCESS

Edited by:
Anurag Krishna,
Swiss Federal Institute of Technology Lausanne, Switzerland

Reviewed by:
Letian Dou,
Purdue University, United States
Noureddine El Messaoudi,
Université Ibn Zohr, Morocco
Mouhaydine Tlemcani,
University of Evora, Portugal

****Correspondence:***
Amal Bouich
ambo1@doctor.upv.es

Specialty section:
This article was submitted to Solar Energy, a section of the journal Frontiers in Energy Research

Received: *21 December 2021*
Accepted: *13 January 2022*
Published: *22 February 2022*

Citation:
Bouich A, Marí-Guaita JA, Sahraoui B, Palacios P and Marí B (2022) Tetrabutylammonium (TBA)-Doped Methylammonium Lead Iodide: High Quality and Stable Perovskite Thin Films. Front. Energy Res. 10:840817. doi: 10.3389/fenrg.2022.840817

HIGHLIGHTS

- The MA(1-X)TBAX PbI3 thin film crystallinity was enhanced with TBA incorporation.
- The morphology of MAPbI3 improved with a pinhole-free surface.
- Optical and PL properties were boosted with the TBA incorporation into MAPbI3 thin film.
- MA(1-X)TBAX PbI3 thin film shows better stability than pure MAPbI3 thin film.

INTRODUCTION

To begin with, nowadays, the Perovskites with formula ABX_3 (A = cation (Formamidinium (FA), Methylammonium (MA).), B = metal cation and X is a halogen anion VII halides (Br^-, Cl^-, I^-)), have been demonstrated good absorbers properties for solar cells with higher photovoltaic conversion efficiency (PCE) (Fakharuddin et al., 2019; Weidman et al., 2019). Methylammonium lead triiodide ($MAPbI_3$) solar cells show good optoelectronic properties with a bandgap between 1.4 and 1.5 eV (Wang et al., 2019), a high absorption coefficient around $10^5 cm^{-1}$ (Im et al., 2011; De Roo et al., 2016) with amazing PCE = 25% (Xiao et al., 2014; Park, 2015). To manufacture $MAPbI_3$ Solar cells, low-cost and simple techniques have been used to deposit the $MAPbI_3$ film: thermal vapor deposition, two-step vapor-assisted deposition (Chen et al., 2013), two-step solution deposition, and one-step solution deposition (Yantara et al., 2015; Patel et al., 2017). Despite the outstanding PCE reported of $MAPbI_3$ solar cells, the problem of $MAPbI_3$ degradation by the loss of MAI and formation of lead

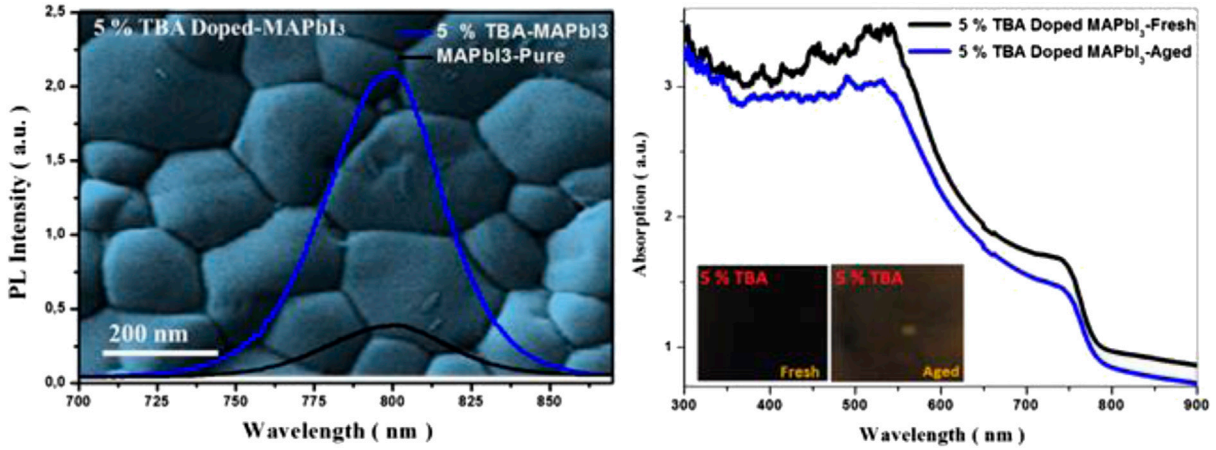

GRAPHICAL ABSTRACT |

iodide PbI_2 under humid conditions and higher temperatures makes use of $MAPbI_3$ difficult (Ko et al., 2015). Concerning to improve the stability of $MAPbI_3$, $MAPbI_3$ was doped by cesium and showed the potential to enhance the stability of $MaPbI_3$ solar cell under UV irradiance conditions (Niu et al., 2016); also on the road for stable $MAPbI_3$, the divalent anion Se^{2-} was incorporated in $MAPbI_3$ structure to increase the atomic interactions between the inorganic and the organic cations (Gong et al., 2018; Li et al., 2018). Considering the ongoing discussion, some researchers have demonstrated that the $MAPbBr_3$ absorber is more stable than $MAPbI_3$; the $MAPbBr_3$ optical absorption is not appropriate for solar cell production (Ahmad et al., 2019).

In this research work, the tetrabutylammonium iodide (TBA) was incorporated into $MAPbI_3$ solution in the form of $MA_{(1-X)}TBA_{(X)}PbI_3$ thin film to study the effect on the structure-property of the $MAPbI_3$ when TBA was incorporated in different percentages. As a result, significant improvement was found in the crystallinity, morphology, optical properties, and stability of the $MA_{(1-X)}TBA_{(X)}PbI_3$ thin film. The obtained results are hoped to help delay the degradation and to enhance the performance of

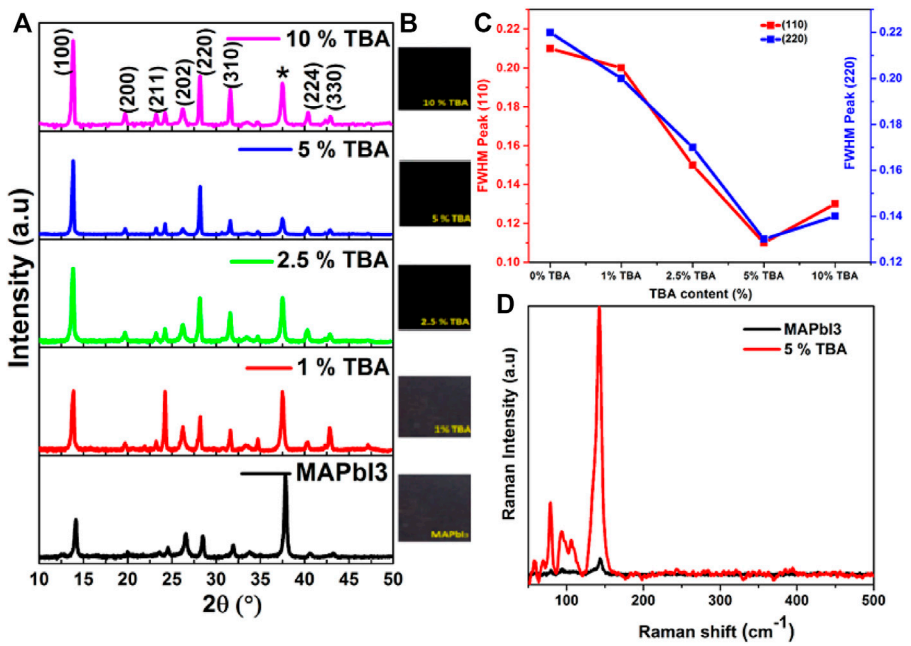

FIGURE 1 | (A) XRD pattern of $MA_{1-x}TBA_xPbI_3$ where X%= (0, 1, 2.5,5, and 10), **(B)** $MA_{1-x}TBA_xPbI_3$ photographs **(C)** FWHM of (011) and (022) peaks of $MA_{1-x}TBA_xPbI_3$ **(C)** Raman spectra of $MAPbI_3$ undoped and doped with 5% TBA.

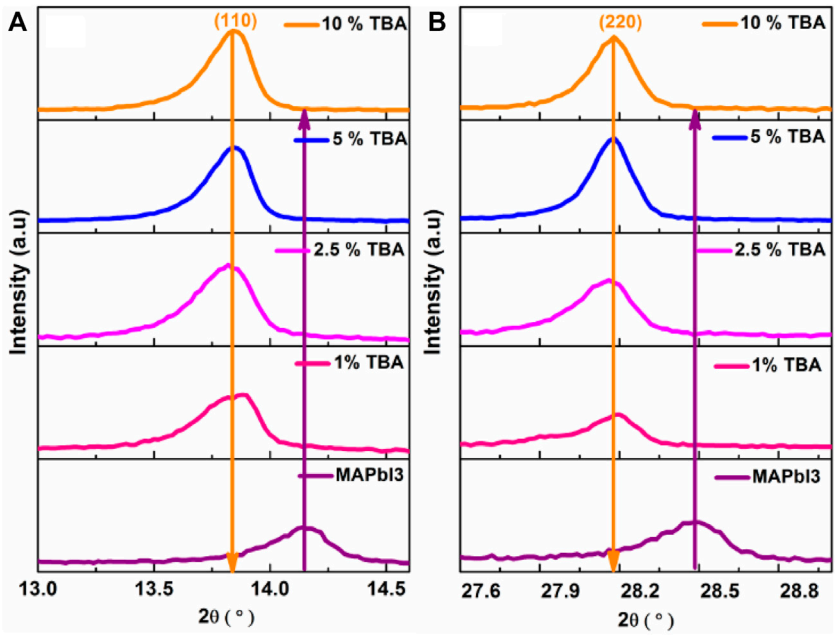

FIGURE 2 | The zoomed XRD peaks, **(A)** (110) and, **(B)** (220) of $MA_{1-x}TBA_xPbI_3$ where X % = (0%, 1%, 2.5%, 5%, and 10%).

TABLE 1 | Lattice parameters of $MA_{1-x}TBA_xPbI_3$ *via* the Pawley method.

Sample. ID	a = b (Å)	c (Å)	Grain size (nm)	Roughness (nm)	Dislocation density (nm^{-1})	Lattice strain (ε)
$MAPbI_3$	8.90	11.12	184.7	147.7	1.04×10^{-05}	0.38
5% TBA	8.91	11.11	249.1	198.5	0.52×10^{-05}	0.39
10% TBA	8.99	11.13	209.8	158.0	0.61×10^{-05}	0.37

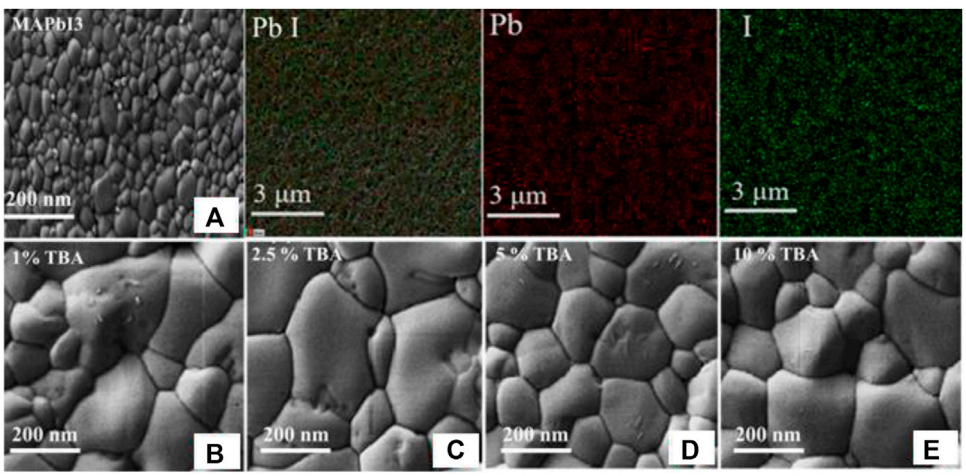

FIGURE 3 | (A) EDS Mapping of $MAPbI_3$ **(B–E)** SEM images of pure and doped $MAPbI_3$.

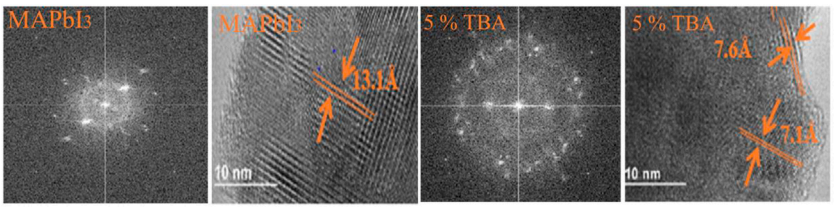

FIGURE 4 | HRTEM Images of undoped and 5% TBA doped $MAPbI_3$.

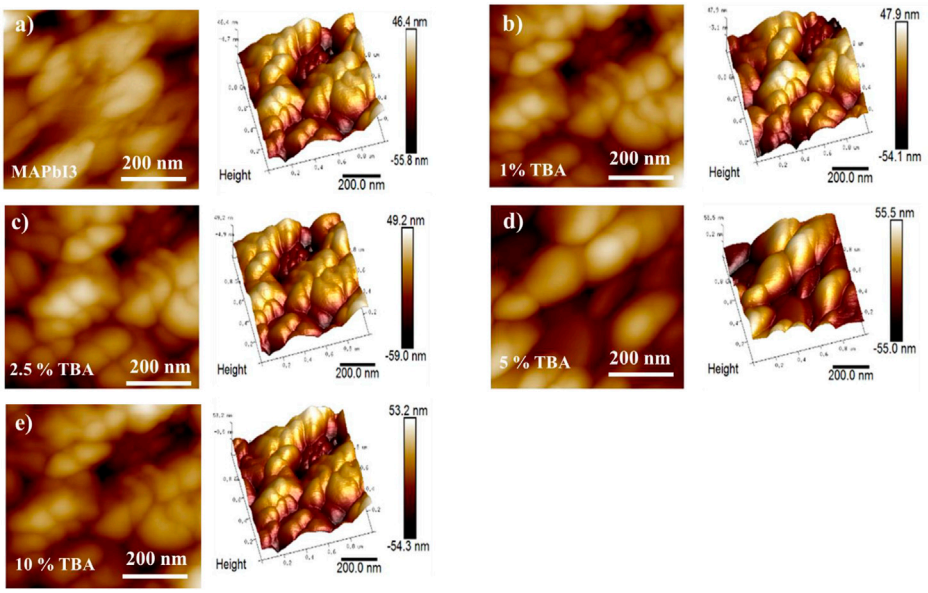

FIGURE 5 | AFM images 2 and 3 Dimensional of pure and doped $MAPbI_3$.

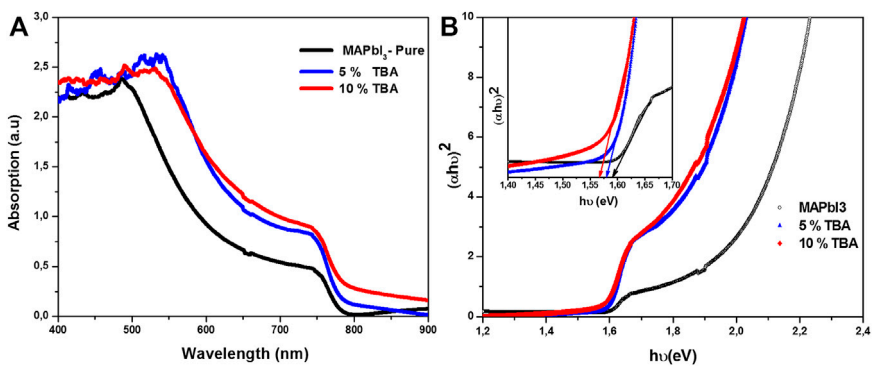

FIGURE 6 | (A) Optical absorption, **(B)** calculated bandgap of $MA_{1-x}TBA_xPbI_3$ where X % = (0%, 5%, and 10%).

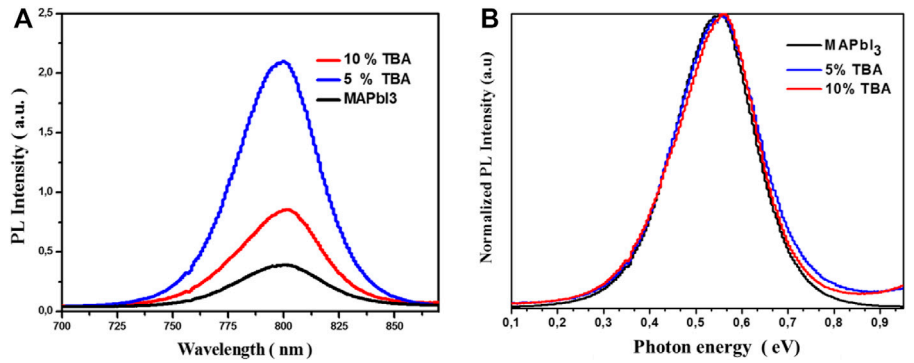

FIGURE 7 | (A) PL spectra and **(B)** is the normalized PL spectra of $MA_{1-x}TBA_xPbI_3$ where X % = (0%, 5%, and 10%) thin film.

TABLE 2 | Band gap variation of $MA_{1-x}TBA_xPbI_3$ where X % = (0%, 5%, and 10%).

Name	Eg from PL		Eg from UV		Stokes shift
	λ (nm)	Eg (eV)	λ (nm)	Eg (eV)	meV
$MAPbI_3$ Pure	778	1.59	752	1.6	220
5% TBA doped	785	1.57	761	1.58	220
10% TBA doped	786	1.56	763	1.56	200

the $MAPbI_3$ thin film by doping TBA cations under ambient conditions.

MATERIALS AND EXPERIMENTAL PROCEDURE

Methylammonium iodide (MAI), Lead (II) iodide (PbI_2), Chlorobenzene (CBZ), Methylammonium iodide (MAI) and Tetrabutylammonium iodide (TBAI), anhydrous N,N-dimethylformamide (DMF) and dimethyl sulfoxide (DMSO). All compounds were purchased from Sigma-Aldrich, and they were used without any additional purification. The $MA_{1-x}TBA_xPbI_3$ solution was prepared in a glovebox by dissolving PbI_2, TBAI, and MAI in the solvent of DMF and DMSO; the solution was agitated at 60°C for 3 h.

CHARACTERIZATION TECHNIQUES

X-ray diffraction (XRD) was employed to characterize the crystallinity of the films using RIGAKU Ultima IV diffractometer the range of 2θ = 10°–60° using CuKa radiation (λ = 1.5418 Å) at room temperature. The morphology characteristic of thin films was constantly observed by scanning electron microscopy (SEM) model (Quanta 200–FEI) under 1.5 kV accelerated potential in several magnifications (Stewart et al., 2021). In addition, the films were examined by atomic force microscopy (AFM) with 0.5Hz a scan rate. The fringes crystallinity was confirmed by Transmission electron microscopy with 2.5 KV. Also, UV-VIS and PL spectra were characterized using Ocean Optics HR4000 spectrophotometer in the range of 300–850 nm and He-Cd laser source Si-CCD detector Hamamatsu for PL analysis, respectively.

RESULTS AND DISCUSSION

In the present work, thin films perovskite $MA_{1-x}TBA_xPbI_3$ were successfully deposited on FTO back contact using a simple spin-coating technique. **Figure 1** shows the XRD results of the $MA_{1-x}TBA_xPbI_3$ where X = (0, 1,2.5, 5, 10). The characteristic peaks located at 14° and 28° match to XRD planes of (110) and (220) respectively in agreement with $MAPbI_3$ structure (Ono et al., 2015; Abdelmageed et al., 2016) without any PbI_2 binary phase. Thus, a significant increase was found in the main XRD peaks (110) and (220) intensities and crystallinity by incorporating the TBA amount. **Figure 2** represents the zoomed XRD peak in the range of 13°–15°; the small shift was observed towards a lower 2θ degree after the incorporation of TBA compared to the $MAPbI_3$ thin film. Furthermore, the increase in the crystal lattice could be related to a bigger radius TBA (4.70 Å) than a small radius of MA (1.8 Å).

The $MAPbI_3$ thin film with a tetragonal structure where a = b = 8.90 Å, c = 11.12 Å and with insignificant changes due to TBA incorporation where a = b = 8.91 Å, c = 11.11 Å. The crystal parameters details of $MA_{1-x}TBA_xPbI_3$ and the grain size were calculated using the Pawley method summarized in **Table 1**. Moreover, FWHM of peaks (110) and (220) values gradually decrease an agreement of good crystallinity of the films with increasing the amount of TBA from 0 to 5% in **Figure 1C**. In this respect, the stability of the $MAPbI_3$ main (110) peak remains excellent after incorporating TBA amounts. Especially many studies have been reported that the inorganized Pb atoms affect the surface imperfections of the film, which leads to a decrease in the performance of perovskite devices. In the current work, the TBA arguably shows a significant improvement of $MAPbI_3$ stability that degrades quickly into PbI_2 in external conditions (Yu et al., 2018).

Here, the Raman spectroscopy analysis was used to verify the phase identification of pure $MAPbI_3$ and 5% doped TBA

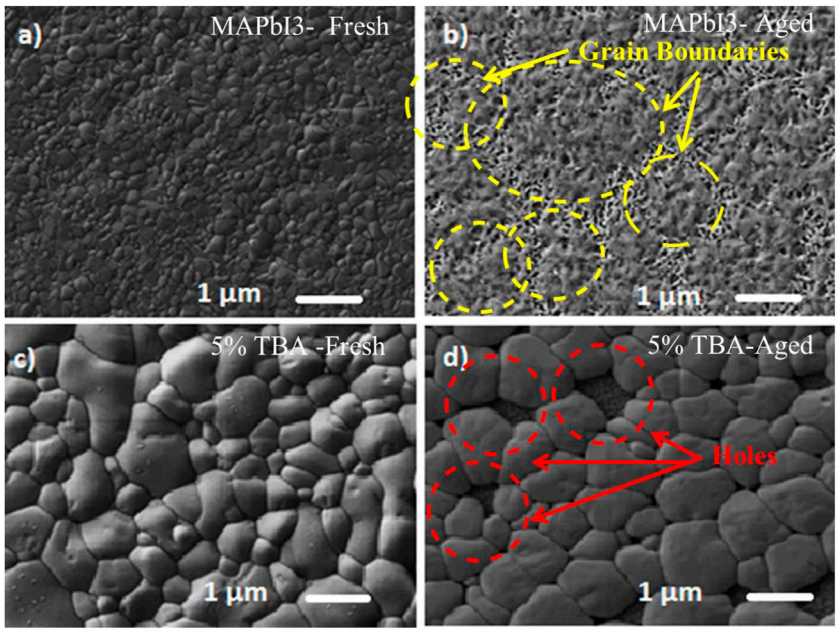

FIGURE 8 | SEM images of Fresh and aged pure and 5% TBA doped $MAPbI_3$ layers.

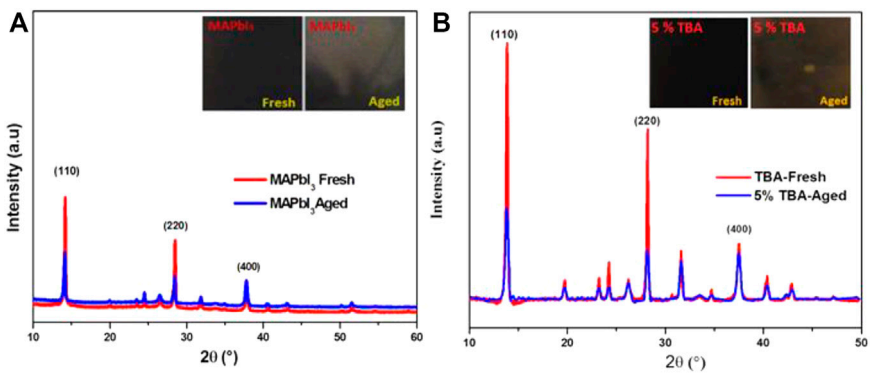

FIGURE 9 | The XRD pattern of fresh and aged $MAPbI_3$ and 5% TBA samples.

Figure 1D. The dominants two vibrational modes were identified for $MAPbI_3$ approximately at 68 cm^{-1} and 142 cm^{-1}. The intensities of the same vibrational mode increased after incorporating 5% TBA content. The 68 and 142 cm^{-1} bands matched with the obtained results from XRD that confirmed the incorporation of TBA, which plays a vital role in the formation of crystallinity (Fateev et al., 2018).

Figure 3 illustrates the SEM images of $MA_{1-x}TBA_xPbI_3$ where X % (0%, 1%, 2.5%, 5%, 10%). The undoped $MAPbI_3$ shows a small grain size with a smooth surface and good distribution of lead and iodide (Chen et al., 2018). In the same way, the TBA incorporation increase gradually grain size of 210 nm for pure $MAPbI_3$, 290 nm for the doped $MAPbI_3$ with 1.0% TBA, 490 nm for 2.50% TBA as well as with a higher value of 500 nm for 5.0% TBA figure (a–d). This improvement of the grain size of doped $MAPbI_3$ can be due to the crystal growth by decreasing crystal nucleation and lead to good surface coverage and higher crystallinity, as shown by the XRD analysis (Banerjee and Chattopadhyay, 2018; Liu et al., 2020). In this connection, the enhanced crystallinity and grain size could be attributed to fewer defects in the trap state, decreasing the non-radiative recombination in the $MAPbI_3$ surface (Guo et al., 2019).

The specimen preparation technique used for perovskite samples prepared is tripod polishing for perovskite for high-resolution TEM investigation, scratching the perovskite film prepared and putting it in the special grid of aluminum to characterize the samples with TEM analysis, **Figure 4** displays TEM analysis of pure $MAPbI_3$ and doped with 5% TBA expose the

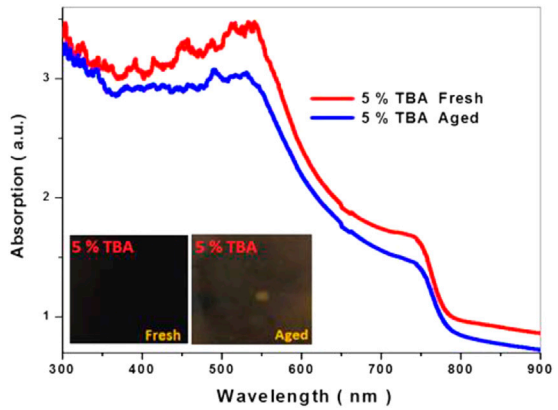

FIGURE 10 | The absorbance of fresh and aged 5% TBA sample.

scattered through lattice fringes spacing of 13.10 Å correspond to [110] crystallographical plan as well as 7.60 Å match with [220] crystallographical respectively. The selected portion of the electron diffraction spectrum shows that pure and 5% TBA doped $MAPbI_3$ films are polycrystalline, where is in good agreement with XRD results (Giesbrecht et al., 2018; Jones et al., 2019).

Figure 5 shows AFM images with 2 and 3 Dimension of undoped and doped $MAPbI_3$, where the measured roughness is varying, that offers a change compared to doped and undoped $MAPbI_3$ where RMS= (147.7, 198, and 168 nm) calculated for the x% TBA where x = (0, 5 and 10) respectively which is measured by the root-mean-square (RMS) (**Table 1**). Moreover, the RMS value of 10% TBA doped $MAPbI_3$ shows a slight decrease than the incorporation of 5% of TBA, showing the optimum level for large grain size and high roughness in the AFM analysis (Tombe et al., 2018).

OPTICAL AND PHOTOLUMINESCENCE STUDY

This experiment performed the optical absorption and photoluminescence measurements for MAPbI3 thin film doped TBA to analyze the optoelectronic properties. Here, **Figure 6A** illustrates the optical absorption of $MAPbI_3$ pure and doped TBA from 400 to 900 nm wavelength, where the optical bandgap was estimated around 1.55–1.59 eV. Upon monitoring carefully, the variation in the optical bandgap was observed by incorporating the TBA amount (Smith et al., 2019). This significant improvement could be related to pinhole-free TBA doped $MAPbI_3$ films, as shown in SEM analysis (Sun et al., 2017).

Besides, **Figure 7** shows the photoluminescence spectrum of undoped $MAPbI_3$ and doped TBA, where the FWHM intensity progressively increases with the increase of TBA content. Doped 5% TBA represents a significantly higher red emission around 55 nm. This emission is three times higher than undoped $MAPbI_3$ thin film. The results could be attributed to reducing trap density states with

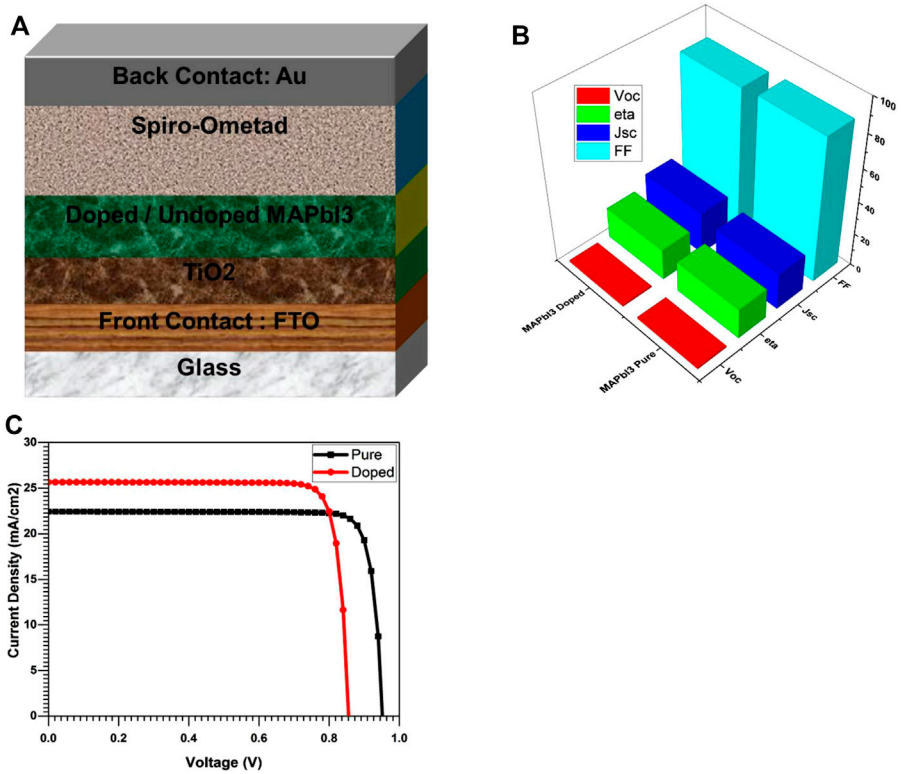

FIGURE 11 | (A) diagram of $MAPbI_3$ based solar cell **(B)** Characteristics Parameters Comparison of MAPbI3 based solar cell **(C)** JV characteristics curves of MAPbI3 based solar cell.

TABLE 3 | Experimental Characteristics Parameters doped and undoped MAPbI3 based solar cell.

Solar cell	Voc	Jsc	FF	Eta
	V	mA/cm2	%	%
Spiro/$MAPbI_3$/TiO_2/F.T.O	0.95	22.4	87.1	18.01
Spiro/$MAPbI_3$:TBA/TiO_2/F.T.O	0.85	25.7	86.1	20.1

decreased charge recombination, which improved the thin film's optoelectronic properties (Brennan et al., 2017; Ngo et al., 2018).

In this context, one of the essential parameters of semiconductor materials is the stokes shift. This shift was observed between the optical absorption edge and PL peak. The comparison of stoke shift values is summarized in **Table 2**. The stoke shift describes the reduction of lattice parameters in the crystals. The low value of the stoke shift indicates the good photophysical properties of $MAPbI_3$ (Bouich et al., 2021a; Bouich et al., 2021b).

DEGRADATION STUDY

The degradation of pure $MAPbI_3$ and 5% doped TBA samples were examined under a dark relative 60% humidity environment where samples were stored for 15 days. Consequently, a significant transformation from the black color to the yellow color was observed for the pure $MAPbI_3$ aged sample after 2 weeks which indicated the dissociation of $MAPbI_3$ to PbI_2 confirmed by yellow color compared to 5% doped TBA aged sample was less affected (**Figure 9**).

Figure 8 illustrates the SEM images of the $MAPbI_3$ surface were affected by humidity and the water molecules over the grain boundaries, which led to the degradation of $MAPbI_3$ and the formation of PbI_2 and MAI. The TBA cation reduced the grain boundaries to prevent the access of humidity into the film. Furthermore, the 5% TBA doped $MAPbI_3$ has shown a slight crystal structure distortion than the pure $MAPbI_3$ (Huang et al., 2017; Kundu and Timothy, 2020).

Figure 9 displays the XRD patterns and the structural variations through the degradation of the doped and undoped $MAPbI_3$ with the characteristic peak (110) of pure $MAPbI_3$ shows dramatically reduced; however, the 5% TBA doped $MAPbI_3$ thin film observed less affected by the environment as compared to pure $MAPbI_3$.

Furthermore, the environmental effect was studied from the UV-Visible analysis of the 5% TBA doped $MAPbI_3$; **Figure 10** shows a slow-down variation in the absorption edge, and the color changed from dark to brown of the sample after 2 weeks in relative humidity (60%). The obtained results confirm that incorporating TBA into the $MAPbI_3$ could decrease the degradation of the methylammonium lead triiodide absorber for photovoltaic application.

Device Spiro/$MAPbI_3$/TiO_2/F.T.O Simulation

As we noticed a change in the bandgap of doped with 5% TBA and undoped MAPbI3 has been observed. The effect of thickness and bandgap variation of the absorber layer has a more significant impact on the performance of solar cells. We simulate a proposed solar cell having a model "Gold/SpiroOmTAD/MAPbI3/TiO2/FTO/Glass" to keep this impact on the cell's performance. Here Gold is used as a front contact, OmTAD as ETL, $MAPbI_3$ as an absorber layer, TiO2 as HTL, F.T.O is working as a back contact, and glass is a substrate (Kundu and Timothy, 2020; Mesbahi et al., 2021; Quan et al., 2019).

Figure 11C show the J-V characteristics curve and clearly show the effect of doped and undoped $MAPbI_3$, Voc was 0.95V, Jsc of 22.4 mA/cm2, FF of 87.1%, and Eta of 18.01% recorded. Here we note that undoped is giving less performance, Voc, Jsc, FF, and Eta were registered as 0.85V, 25.7 mA/cm2, 86.1%, and 20.42%, respectively, which was good as compared to the results of the film growth and crystallinity (**Table 3** and **Table.1** in **Supplementary Materials**).

CONCLUSION

To sum up, from the preceding discussion, it appears that the doped with a small amount of TBA significantly increases the morphology and stability of $MAPbI_3$ thin film for photovoltaic applications. The XRD analysis revealed that the crystallinity of $MAPbI_3$ thin film enhanced with TBA, the TBA affects leading $MAPbI_3$ film with a homogenous, highly rough surface and large grain size, which could cause trap more light in the surface. Similarly, the $MA_{(1-X)}TBA_XPbI_3$ thin film shows better stability in a relative humidity of ~60% after 15 days than pure $MAPbI_3$ thin film. The obtained results are hoped to help delay the degradation and to enhance the performance of the $MAPbI_3$ thin film by doping TBA cations under ambient conditions.

DATA AVAILABILITY STATEMENT

The original contributions presented in the study are included in the article/**Supplementary Material**, further inquiries can be directed to the corresponding author.

AUTHOR CONTRIBUTIONS

Conceptualization AB; methodology, AB; validation BS formal analysis, JM-G; investigation PP resources AB data curation, AB; writing—original draft preparation, JM-G; writing—review and editing, AB, BM; visualization, AB; supervision, BM; project administration, funding acquisition, BM. All authors have read and agreed to the published version of the manuscript.

FUNDING

This work was supported by the Ministerio de Economia y Competitividad (ENE 2016-77798-C4-2-R). Author AB acknowledged the Post-doctoral contract supported by the

RRHH, the Postdoctoral contract the Margarita Salas financed with union European Next Generation EU. Grant PID2019-107137RB-C21 and PID2019-107137RB-C22OAQ funded by MCIN/AEI/10.13039/501100011033 and by "ERDF A way of making Europe.

REFERENCES

Abdelmageed, G., Jewell, L., Hellier, K., Seymour, L., Luo, B., Bridges, F., et al. (2016). Mechanisms for Light Induced Degradation in MAPbI3 Perovskite Thin Films and Solar Cells. *Appl. Phys. Lett.* 109 (23), 233905. doi:10.1063/1.4967840

Ahmad, Z., Shikoh, A. S., Paek, S., Nazeeruddin, M. K., Al-Muhtaseb, S. A., Touati, F., et al. (2019). Degradation Analysis in Mixed (MAPbI3 and MAPbBr3) Perovskite Solar Cells under thermal Stress. *J. Mater. Sci. Mater. Electron.* 30 (2), 1354–1359. doi:10.1007/s10854-018-0403-4

Banerjee, D., and Chattopadhyay, K. K. (2018). "Hybrid Inorganic Organic Perovskites," in *Perovskite Photovoltaics* (Academic Press), 123–162. doi:10.1016/b978-0-12-812915-9.00005-8

Bouich, A., Ullah, S., Marí, B., Atourki, L., and Touhami, M. E. (2021a). One-step Synthesis of FA1-xGAxPbI3 Perovskites Thin Film with Enhanced Stability of Alpha (α) Phase. *Mater. Chem. Phys.* 258, 123973. doi:10.1016/j.matchemphys.2020.123973

Bouich, A., Mari, B., Atourki, L., Ullah, S., and Touhami, M. E. (2021b). Shedding Light on the Effect of Diethyl Ether Antisolvent on the Growth of (CH3NH3) PbI3 Thin Films. *JOM* 73 (2), 551–557. doi:10.1007/s11837-020-04518-5

Brennan, M. C., Zinna, J., and Kuno, M. (2017). Existence of a Size-dependent Stokes Shift in CsPbBr3 Perovskite Nanocrystals. *ACS Energ. Lett.* 2 (7), 1487–1488. doi:10.1021/acsenergylett.7b00383

Chen, L.-C., Lee, K.-L., Wu, W.-T., Hsu, C.-F., Tseng, Z.-L., Sun, X. H., et al. (2018). Effect of Different CH3NH3PbI3 Morphologies on Photovoltaic Properties of Perovskite Solar Cells. *Nanoscale Res. Lett.* 13 (1), 140. doi:10.1186/s11671-018-2556-8

Chen, Q., Zhou, H., Hong, Z., Luo, S., Duan, H.-S., Wang, H.-H., et al. (2013). Planar Heterojunction Perovskite Solar Cells via Vapor-Assisted Solution Process. *J. Am. Chem. Soc.* 136 (2), 622–625. doi:10.1021/ja411509g

De Roo, J., Ibáñez, M., Geiregat, P., Nedelcu, G., Walravens, W., Maes, J., Martins, J. C., Van Driessche, I., Kovalenko, M. V., and Hens, Z. (2016). Highly Dynamic Ligand Binding and Light Absorption Coefficient of Cesium lead Bromide Perovskite Nanocrystals. *ACS Nano* 10 (2), 2071–2081. doi:10.1021/acsnano.5b06295

Fakharuddin, A., Shabbir, U., Qiu, W., Iqbal, T., Sultan, M., Heremans, P., et al. (2019). Inorganic and Layered Perovskites for Optoelectronic Devices. *Adv. Mater.* 31 (47), 1807095. doi:10.1002/adma.201807095

Fateev, S. A., Petrov, A. A., Khrustalev, V. N., Dorovatovskii, P. V., Zubavichus, Y. V., Goodilin, E. A., et al. (2018). Solution Processing of Methylammonium Lead Iodide Perovskite from γ-Butyrolactone: Crystallization Mediated by Solvation Equilibrium. *Chem. Mater.* 30 (15), 5237–5244. doi:10.1021/acs.chemmater.8b01906

Giesbrecht, N., Schlipf, J., Grill, I., Rieder, P., Dyakonov, V., Bein, T., et al. (2018). Single-crystal-like Optoelectronic-Properties of MAPbI3 Perovskite Polycrystalline Thin Films. *J. Mater. Chem. A.* 6 (11), 4822–4828. doi:10.1039/c7ta11190h

Gong, J., Yang, M., Rebollar, D., Rucinski, J., Liveris, Z., Zhu, K., et al. (2018). Divalent Anionic Doping in Perovskite Solar Cells for Enhanced Chemical Stability. *Adv. Mater.* 30 (34), 1800973. doi:10.1002/adma.201800973

Guo, P., Ye, Q., Yang, X., Zhang, J., Xu, F., Shchukin, D., and Wang, H. (2019). Surface & Grain Boundary Co-passivation by Fluorocarbon-Based Bifunctional Molecules for Perovskite Solar Cells Efficiency over 21%. *J. Mater. Chem. A* 7 (6), 2497–2506. doi:10.1039/c8ta11524a

Huang, J., Tan, S., Lund, P. D., and Zhou, H. (2017). Impact of H_2O on Organic-Inorganic Hybrid Perovskite Solar Cells. *Energ. Environ. Sci.* 10 (11), 2284–2311. doi:10.1039/c7ee01674c

Im, J. H., Lee, C. R., Lee, J. W., Park, S. W., and Park, N. G. (2011). 6.5% Efficient Perovskite Quantum-Dot-Sensitized Solar Cell. *Nanoscale* 3 (10), 4088–4093. doi:10.1039/c1nr10867k

Jones, T. W., Osherov, A., Alsari, M., Sponseller, M., Duck, B. C., Jung, Y.-K., et al. (2019). Lattice Strain Causes Non-radiative Losses in Halide Perovskites. *Energy Environ. Sci.* 12 (2), 596–606. doi:10.1039/c8ee02751j

Ko, H. S., Lee, J. W., and Park, N. G. (2015). 15.76% Efficiency Perovskite Solar Cells Prepared under High Relative Humidity: the Importance of PbI_2 Morphology in Two-step Deposition of CH_3 NH_3 PbI_3. *J. Mater. Chem. A* 3 (16), 8808–8815. doi:10.1039/c5ta00658a

Kundu, S., and Timothy, L. K. (2020). *In Situ* studies of the Degradation Mechanisms of Perovskite Solar Cells. *EcoMat* 2 (2), e12025. doi:10.1002/eom2.12025

Li, J., Jiu, T., Duan, C., Wang, Y., Zhang, H., Jian, H., et al. (2018). Improved Electron Transport in MAPbI3 Perovskite Solar Cells Based on Dual Doping Graphdiyne. *Nano Energy* 46, 331–337. doi:10.1016/j.nanoen.2018.02.014

Liu, C., Cheng, Y.-B., and Ge, Z. (2020). Understanding of Perovskite crystal Growth and Film Formation in Scalable Deposition Processes. *Chem. Soc. Rev.* 49 (6), 1653–1687. doi:10.1039/c9cs00711c

Marí-Guaita, J., Bouich, A., Shafi, M. A., Bouich, A., and Marí, B. Investigation on the stability and efficiency of MAPbI3 and MASnI3 thin films for Solar Cells. *Physica Status Solidi (a)*

Mesbahi, O., Tlemçani, M., Janeiro, F. M., Hajjaji, A., and Kandoussi, K. (2021). Sensitivity Analysis of a New Approach to Photovoltaic Parameters Extraction Based on the Total Least Squares Method. *Metrology Meas. Syst.*,28 751–765. doi:10.24425/mms.2021.137707

Ngo, T. H., Gil, B., Shubina, T. V., Damilano, B., Vezian, S., Valvin, P., et al. (2018). Enhanced Excitonic Emission Efficiency in Porous GaN. *Sci. Rep.* 8 (1), 15767–15769. doi:10.1038/s41598-018-34185-1

Niu, G., Yu, H., Li, J., Wang, D., and Wang, L. (2016). Controlled Orientation of Perovskite Films through Mixed Cations toward High Performance Perovskite Solar Cells. *Nano Energy* 27, 87–94. doi:10.1016/j.nanoen.2016.06.053

Ono, L. K., Raga, S. R., Remeika, M., Winchester, A. J., Gabe, A., and Qi, Y. (2015). Pinhole-free Hole Transport Layers Significantly Improve the Stability of MAPbI3-Based Perovskite Solar Cells under Operating Conditions. *J. Mater. Chem. A.* 3 (30), 15451–15456. doi:10.1039/c5ta03443d

Park, N.-G. (2015). Perovskite Solar Cells: an Emerging Photovoltaic Technology. *Mater. Today* 18 (2), 65–72. doi:10.1016/j.mattod.2014.07.007

Patel, J. B., Wong-Leung, J., Van Reenen, S., Sakai, N., Wang, J. T. W., Parrott, E. S., et al. (2017). Influence of Interface Morphology on Hysteresis in Vapor-Deposited Perovskite Solar Cells. *Adv. Electron. Mater.* 3 (2), 1600470. doi:10.1002/aelm.201600470

Quan, L. N., Rand, B. P., Friend, R. H., Mhaisalkar, S. G., Lee, T.-W., and Sargent, E. H. (2019). Perovskites for Next-Generation Optical Sources. *Chem. Rev.* 119 (12), 7444–7477. doi:10.1021/acs.chemrev.9b00107

Smith, M. D., Connor, B. A., and Karunadasa, H. I. (2019). Tuning the Luminescence of Layered Halide Perovskites. *Chem. Rev.* 119 (5), 3104–3139. doi:10.1021/acs.chemrev.8b00477

Stewart, A. W., Bouich, A., and Soucase, B. M. (2021). Enhancing the stability and crystallinity of $CsPbIBr_2$ through antisolvent engineering. *J. Mater. Sci.* 56 (36), 20071–20086.

Sun, C., Guo, Y., Fang, B., Guan, L., Duan, H., Chen, Y., et al. (2017). Facile Preparation of High-Quality Perovskites for Efficient Solar Cells via a Fast Conversion of Wet PbI2precursor Films. *RSC Adv.* 7 (36), 22492–22500. doi:10.1039/c7ra03066e

Tombe, S., Adam, G., Heilbrunner, H., Yumusak, C., Apaydin, D. H., Hailegnaw, B., et al. (2018). The Influence of Perovskite Precursor Composition on the Morphology and Photovoltaic Performance of Mixed Halide MAPbI3-xClx Solar Cells. *Solar Energy* 163, 215–223. doi:10.1016/j.solener.2018.01.083

Wang, Y., Fang, W.-H., Long, R., and Prezhdo, O. V. (2019). Symmetry Breaking at MAPbI3 Perovskite Grain Boundaries Suppresses Charge Recombination:

SUPPLEMENTARY MATERIAL

The Supplementary Material for this article can be found online at: https://www.frontiersin.org/articles/10.3389/fenrg.2022.840817/full#supplementary-material

Time-Domain Ab Initio Analysis. *J. Phys. Chem. Lett.* 10 (7), 1617–1623. doi:10.1021/acs.jpclett.9b00763

Weidman, M. C., Seitz, M., and Tisdale, W. A. (2019). *U.S. Patent No. 10,273,405* (Washington, DC: U.S. Patent and Trademark Office).

Xiao, Z., Bi, C., Shao, Y., Dong, Q., Wang, Q., Yuan, Y., et al. (2014). Efficient, High Yield Perovskite Photovoltaic Devices Grown by Interdiffusion of Solution-Processed Precursor Stacking Layers. *Energ. Environ. Sci.* 7 (8), 2619–2623. doi:10.1039/c4ee01138d

Yantara, N., Sabba, D., Yanan, F., Kadro, J. M., Moehl, T., Boix, P. P., et al. (2015). Loading of Mesoporous Titania Films by CH3NH3PbI3 Perovskite, Single Step vs. Sequential Deposition. *Chem. Commun.* 51 (22), 4603–4606. doi:10.1039/c4cc09556a

Yu, W., Yu, S., Zhang, J., Liang, W., Wang, X., Guo, X., et al. (2018). Two-in-one Additive-Engineering Strategy for Improved Air Stability of Planar Perovskite Solar Cells. *Nano Energy* 45, 229–235. doi:10.1016/j.nanoen.2017.12.041

Conflict of Interest: The authors declare that the research was conducted in the absence of any commercial or financial relationships that could be construed as a potential conflict of interest.